Atomic Spectroscopy

Article

In-situ Sulfur Isotopic Analysis of Sulfate by Laser Ablation Multiple Collector Inductively Coupled Plasma Mass Spectrometry (LA-MC-ICP-MS)

Jue Lu,[a] Wei Chen,[a,*] Shao-Yong Jiang,[a] Kui-Dong Zhao,[a] Antonio Simonetti,[b] and Dao-Hui Pi[a]

[a] State Key Laboratory of Geological Processes and Mineral Resources, Collaborative Innovation Center for Exploration of Strategic Mineral Resources, Faculty of Earth Resources, P.R. China University of Geosciences, Wuhan, 430074, P.R. China

[b] University of Notre Dame, Department of Civil and Environmental Engineering and Earth Sciences, South Bend, IN 46556, USA

Received: *October 15, 2020;* ***Revised:*** *October 31, 2020;* ***Accepted:*** *October 31, 2020;* ***Available online:*** *November 27, 2020*

DOI: 10.46770/AS.2020.208

ABSTRACT: Sulfate minerals are widely distributed in nature, and their sulfur isotopic signatures offer a largely untapped source of potential information for improving our understanding of magmatic, hydrothermal, and sedimentary processes. In this study, we describe an analytical procedure for measuring the sulfur isotopic compositions of natural sulfate-bearing samples using a LA-MC-ICP-MS (laser ablation multiple collector inductively coupled plasma mass spectrometry) technique. YF-2 barite ($BaSO_4$) from the Yongfu hydrothermal deposit yields a $\delta^{34}S$ value of 18.1 ± 0.4‰ (n = 11, 2SD), obtained by elemental analyzer-isotope ratio mass spectrometry (EA-IRMS), and has been adopted as the reference material for sulfur isotopic determination in this study. The sulfur isotopic ratios for NBS 127 and IAEA-SO-5 barium sulfate are validated by using YF-2 pressed powder tablets as the internal reference standard, and this analytical protocol yielded results that overlap with recommended values. The $\delta^{34}S$ values obtained here for the YF-1, GTS, and DGD barites are similar to those recorded by EA-IRMS for these samples. WC barite displays highly variable sulfur isotopic compositions, although the average $\delta^{34}S$ value for WC barite is similar to that obtained by EA-IRMS. Sulfates in the barite-celestine solid solution series and anhydrite were analyzed to determine the isotopic fractionation in varied matrices using both the RESOlution and GeoLasHD laser ablation systems. The analytical results suggest minimal sulfur isotopic fractionation between barite and other S-bearing matrices using both laser systems. For non-matrix matched sulfur isotope analysis, the ion signal intensity and laser parameters are important parameters that must be closely monitored. If sulfur isotopic fractionation is observed during sample ablation, this feature can be minimized by employing a smaller beam size, lower repetition rate and fluence output.

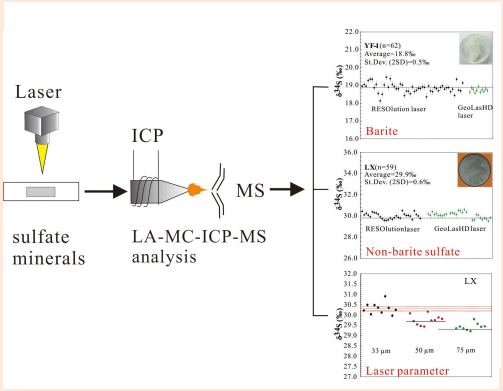

INTRODUCTION

Sulfur (S) is prevalent in the natural environment and S-bearing minerals form over the entire temperature range of geological interest: from low temperature surficial processes associated with the evaporation of seawater to form evaporite deposits, to high temperature magmatic-hydrothermal processes associated with the formation of basic and precious metal deposits.[1] Investigation of sulfur isotopic compositions (expressed in terms of per mil deviation as $\delta^{34}S$) is useful for unraveling the geochemical history of geological and biological systems with particular interest in the isotopic variation among sulfide and sulfate minerals.[2] Naturally occurring sulfide and sulfate minerals are characterized by $\delta^{34}S$ values that range from − 60 to +30‰, which may provide reliable information on the origin of sulfur and its terrestrial cycle.[3] The sulfur isotopic fractionation between sulfide and sulfate has been used to establish the oxidation state at a given

temperature during their respective formations (*e.g.* Marini *et al*.[4]). Sulfur isotopic compositions can change significantly within a single complex or sample. For instance, multiple sulfur isotopic compositions for porewater sulfate from Mangrove Lake (Bermuda) are indicative of fractionation during redox sulfur cycling.[5]

High precision sulfur isotope ratios were conventionally determined by gas source isotope ratio mass spectrometry (GS-IRMS) with a precision better than 0.05‰ using either SO_2 or SF_6 gas.[6,7] EA-IRMS (elemental analyzer-isotope ratio mass spectrometry) is the most commonly used analytical method for the determination of sulfur isotope ratios for sulfate-bearing samples due to its simple preparation, efficiency, accuracy, and precision.[2,8,9] Recent geological studies have focused on investigating the isotopic composition of sulfur-bearing samples at high spatial resolution to track crystal growth, zonation and fluid evolution during mineral crystallization. For example, in-situ sulfur isotopic measurement by laser ablation (LA) MC-ICP-MS has recently been further developed, especially in relation to the investigation of sulfides.[10–19] Most of the barite present in the Earth's crust forms through the mixing of fluids from diverse origins, including magmatic,[20] metamorphic,[21] hydrothermal,[22] as well as ancient and modern ocean water.[23] The micron scale sulfur isotopic composition of barite and other related sulfates could definitely provide important information regarding their origin and formation history (*e.g.* redox condition, pH and temperature). In line with the most recent developments for sulfur isotopic analysis of sulfide and sulfate, this work aims to provide a detailed investigation of in-situ sulfur isotopic determination for natural sulfate-bearing minerals by LA-MC-ICP-MS.

Instrumental mass bias is an important potential source of uncertainty in relation to precision and accuracy when measuring light elemental isotopic compositions using MC-ICP-MS. Mason *et al*.[19] combined an external standard liquid aerosol to its laser-produced counterpart to correct the instrumental mass bias using the observed mass bias of either $^{37}Cl/^{35}Cl$ or $^{30}Si/^{29}Si$. Craddock *et al*.[12] introduced laser aerosol to the cyclonic spray dual chamber that was mixed with 2% HNO_3 solution, then calibrated with a matrix-matched solution standard to correct the mass bias. In recent studies, Sample-Standard-Bracketing (SSB) is the most popular approach to monitor and correct sulfur isotope mass bias using LA-MC-ICP-MS.[11,16–18,24–28] SSB monitors both the mass bias within the MC-ICP-MS instrument and the laser-induced isotopic fractionation at the ablation site. This approach requires an appropriately matrix-matched solid standard, which can be natural minerals, pressed powder tablets, or other types of artificial solid samples.[16,26,29,30] A single bracketing standard works for the sulfur isotope characterization of sulfide using SSB,[17,27,28] whereas different sulfate minerals behave differently as the isotopic composition of the sample and bracketing standard is recommended to be matched.[16] National Institute of Standards and Technology (NIST) and United States Geological Survey (USGS) sulfate isotope reference materials have been adopted in previous investigations using MC-ICP-MS.[13,16,19] Currently, no natural sulfate mineral standard is routinely available for in-situ sulfur isotopic analysis.

In this study, we present an analytical procedure using a natural barite (YF-2) as the reference material for sulfur isotopic ratio determination by LA-MC-ICP-MS. This approach offers a further step towards tapping into the wealth of small-scale information locked in barite (and other sulfates) and reflects the complicated hydrothermal and magmatic history for sulfur-related geological systems. Varied matrices can lead to inaccurately measured values if there are differences between the behavior of the samples and the reference materials during the laser ablation process. Thus, we also present sulfur isotope data for a selection of sulfate minerals across a range of lithologies that are purposely matrix mismatched relative to the YF-2 barite reference standard.

EXPERIMENTAL

Samples. The sulfate samples adopted for this study include the NBS 127 (NIST SRM 8557) and IAEA-SO-5 barium sulfate standards, hydrothermal and magmatic barites from the Yongfu (Guangxi) and Wuchuan (Guizhou) barite deposits, and Mianning-Dechang carbonatite complexes (Sichuan). In addition, the isomorphic series of minerals, such as barytocelestine from the Huanglongpu carbonatite-related rare earth element (REE)-Mo deposit (Shanxi), celestine from the Bayan Khushu REE deposit (Mongolia), and anhydrite from Lingxiang Iron Ore (Hubei) have been selected to test and validate the analytical method adopted here; in particular to evaluate the isotopic fractionation among varied compositions of sulfates. Barites from the Yongfu (YF-1 and YF-2) and Wuchuan (WC) hydrothermal deposits occur as fragile aggregates of white or colorless large crystals (up to 1 cm long). Barite from the Mianning-Dechang REE deposits (including DGD and GTS) is pale yellow and may contain minor inclusions of fluorite. The $\delta^{34}S$ values for barite from the DGD deposit were reported by Tian *et al*.[31] and range from 3.3−5.9‰. Barytocelestine from the Huanglongpu carbonatite-related REE-Mo deposit forms fragile light brown rhombic crystals. This barytocelestine is characterized by a $\delta^{34}S$ value of 4.6−5.1‰.[32] Celestine from the Bayan Khushu (BK) carbonatite complex is light blue in color and transparent.

Approximately 0.3 g each of pulverized NBS 127 and IAEA-SO-5 barium sulfate standards and YF-2 barite powder

(binder-free) was set into a PVC ring (~ 1 cm in diameter) and pressed into tablets using a tablet press at 300 kN (~1 × 10^6 kPa) of pressure. These tablets were mounted independently onto a smooth and clean transparent sheet in epoxy resin, then were polished with 2 mm diamond paste to give a flat surface suitable for laser ablation. All of the natural mineral crystals were made into one inch-sized round targets, which were fixed by epoxy resin.

Bulk sulfur isotopic determination. Bulk sulfate mineral separates were powdered to 200 mesh for sulfur isotopic determination by using a Thermo Fisher Scientific Delta V Plus isotope ratio mass spectrometer coupled to a Flash elemental analyzer (EA-IRMS), located at the State Key Laboratory of Biogeology and Environmental Geology (BEG), China University of Geosciences (Wuhan). The samples and the standards were weighed into tin capsules. V_2O_5 was added as an oxidation catalyst in an amount approximately twice the weight of the sample. The tin capsules of the samples and the standards were closed, crushed to a small size and loaded into an AS 200 autosampler (Fisons Instruments). They were flash-combusted sequentially under a stream of helium and oxygen at 1050 °C in a single oxidation-reduction quartz tube filled with high purity oxidizing (tungsten trioxide, WO_3) and reducing (elemental Cu) agents. The combustion-derived gases (SO_2, SO, H_2O, CO_2, N_2) were first dried by passing them through a 10 cm long column filled with anhydrous $Mg(ClO_4)_2$, then directed through a 0.8 m PTFE chromatographic column packed with Porapack 50−80 mesh (Fisons Instruments) at 70 °C for the separation of SO_2, which was isotopically analyzed by IRMS. Pure SO_2 gas was inserted into the He carrier flow as pulses of reference gas. Sulfur isotope ratios are reported in standard δ-notation relative to Vienna Canon Diablo Troilite (V-CDT)[33] using the following expression:

$$\delta^{34}S_{V\text{-}CDT}=\left[\left({}^{34}S/{}^{32}S\right)_{sample}/\left({}^{34}S/{}^{32}S\right)_{standard}\text{-}1\right]\times 1000$$

where the $^{34}S/^{32}S$ ratio of the standard is normalized for V-CDT with the value of 0.044163.[34] The analytical precision for $\delta^{34}S$ of the sample set, based on the replicate analyses of NBS 127 ($\delta^{34}S$ = 20.3‰)[19] and the International Atomic Energy Agency (IAEA) barium sulfate reference materials (IAEA-SO-5, $\delta^{34}S$ = 0.5‰ and IAEA-SO-6, $\delta^{34}S$ = −34.1‰; from the IAEA reference material certificates), was approximately ± 0.4‰ (2SD level).

The sulfur isotopic values of several barites (YF-2, YF-1 and WC) and non-barite sulfates were verified at the Institute of Geographic Sciences and Natural Resources Research, Chinese Academy of Sciences (IGSNRR, CAS). The non-barite sulfates (celestine, barytocelestine and anhydrite) were converted to barium sulfate ($BaSO_4$). 30 mg of celestine, barytocelestine and anhydrite were first dissolved in a solution of 50 mmol L^{-1} of Diethylene Triamine Pentacetic Acid (DTPA) by heating in a water bath, then acidified with HCl to pH < 2. Subsequently, approximately 25 mL of 8.5% $BaCl_2$ solution was added to quantitatively precipitate barium sulfate. The sulfur isotope measurements of barite and converted barium sulfate were performed using an EA coupled to a Delta V Advantage IRMS. The long-term reproducibility of the measurements was better than 0.4‰ (2SD level).[35]

Table 1. Instrumental Parameters for the Laser Ablation System and MC-ICP-MS

Laser		
Laser	RESOlution 193 nm Laser	GeoLasHD 193 nm Laser
Carrier gas	Helium	Helium
Spot size	33−90 μm	32−90 μm
Ablation duration (analysis time)	40 s	40 s
Pulse rate	4−16 Hz	5−15 Hz
Energy density	3−17.8 J cm^{-2}	3−16 J cm^{-2}
Pulse length	20 ns	25 ns
Laser "carrier" gas	0.3–0.4 L min^{-1}, He	0.8 L min^{-1}, He
Mass spectrometer		
MC-ICP-MS	Nu plasma II	
RF power	1300 W	
Cooling gas	13.5 L min^{-1}, Ar	
Auxiliary gas	0.68 L min^{-1}, Ar	
Sample gas	0.55−0.65 L min^{-1}, Ar	
Nitrogen	0.004 L min^{-1}	

In-situ sulfur isotopic determination. In-situ sulfur isotope ratio measurements were performed using two 193 nm ArF excimer laser ablation systems, including the RESOlution laser (Australian Scientific Instruments, Canberra Australia) with a two-volume laser-ablation cell (Laurin Technic, Australia) and the GeoLasHD laser (Coherent, Germany) with a round sample cell. Both laser systems were coupled to a Nu Plasma II multi-collector (MC) ICP-MS (Nu Instruments, U.K.) at the State Key Laboratory of Geological Processes and Mineral Resources (GPMR), China University of Geosciences (Wuhan). The pulse lengths are 20 and 25 ns for the RESOlution and GeoLasHD lasers, respectively. The Nu Instruments Plasma II features 16 fixed Faraday cups to maximize the number and range of the isotopes analyzed. The instrumental settings and typical operating parameters are summarized in Table 1. A series of laser parameters were used for the investigation of laser-induced matrix effects. Beam diameters between 33 μm and 75 μm with corresponding fluences of 4.5−17.8 J cm^{-2} and repetition rates of 4−16 Hz were used with the RESOlution laser. For analysis of the pressed powder tablets, both a relatively low fluence and frequency were used in conjunction with a small spot size (2 J cm^{-2}; 4 Hz and 33 μm). In contrast, a beam size between 32 μm and 90 μm, frequency of 5−15 Hz and fluence of 3−16 J

Table 2. Isobaric (spectral) Interferences on Sulfur Isotope Masses

Isotope	Abundance (%)[a]	Interference
^{32}S	94.99	$^{16}O - ^{16}O$
		$^{14}N - ^{18}O$
		$^{15}N - ^{16}O - ^{1}H$
		$^{14}N - ^{16}O - ^{1}H - ^{1}H$
^{33}S	0.75	$^{17}O - ^{16}O$
		$^{32}S - ^{1}H$
		$^{16}O - 1^{6}O - ^{1}H$
		$^{14}N - ^{18}O - ^{1}H$
		$^{15}N - ^{18}O$
^{34}S	4.25	$^{18}O - ^{16}O$
		$^{33}S - ^{1}H$
		$^{32}S - ^{1}H - ^{1}H$
		$^{16}O - ^{17}O - ^{1}H$
		$^{16}O - ^{16}O - ^{1}H - ^{1}H$
		$^{15}N - ^{18}O - ^{1}H$
^{36}S	0.01	^{36}Ar

cm^{-2} were used with the GeoLasHD laser. The samples were ablated in a He atmosphere, and the particulates produced (He gas) were then combined with additional Ar (0.6 L min^{-1}) before entering the plasma torch. The ion signals for ^{34}S, ^{33}S and ^{32}S were measured simultaneously. The data were obtained in time-resolved analysis (TRA) mode for all laser-introduced samples. YF-2 barite was used as the primary reference material to correct for instrumental mass bias. Three to five samples were analyzed between each set of standards. Each sample acquisition consisted of 30 s of an on-peak background measurement, 40 s of ablation data acquisition and 50 s of washout. The typical background intensity for ^{32}S on the MC-ICP-MS was 0.2−0.5 V, with the sample resulting in a signal response of 3−25 V depending on the laser ablation spot size, laser frequency, and fluence.

RESULTS AND DISCUSSION

Peak shape. The polyatomic interferences created by various isotopes of oxygen dimers cause major spectral interferences on ^{32}S and ^{33}S using the MC-ICP-MS technique. Polyatomic interferences are believed to be lower when a laser ablation introduction system is used compared to the solution mode analysis since the latter introduces additional oxygen and hydrogen originating from the H_2O (and dilute HNO_3) matrix.[15] The potential interfering species on sulfur isotopes are listed in Table 2. Due to the low abundance of ^{36}S (only 0.017%) and the major interference of ^{36}Ar on ^{36}S, this isotope was not investigated. Previous investigations have demonstrated that analyses conducted in high resolution mode (i.e., mass resolving power > 5000) result in an interference-free shoulder on the low-mass side of the ^{32}S peak.[12,25] For Nu Plasma instruments, Pribil *et al.*[16] illustrated that the pseudo medium resolution mode (the mass resolution number ~ 3000) resulted in a satisfactory shoulder-free interference with 2.5

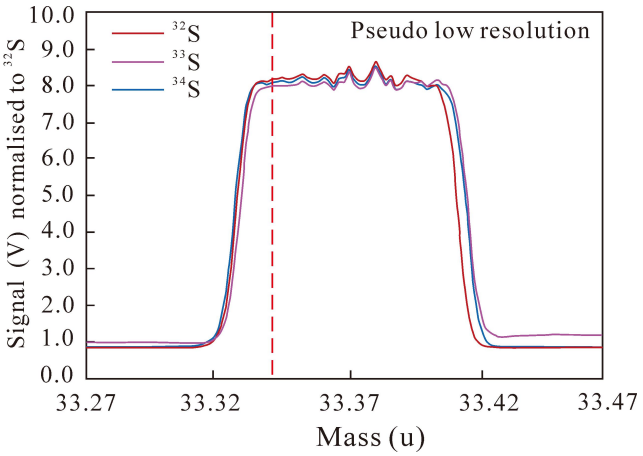

Fig. 1 Mass scan for the three sulfur isotopes (^{32}S, ^{33}S, ^{34}S). The red dotted line represents the plateau position at which isotopic ratios are measured.

times more signal compared to the pseudo high resolution mode. Hence, generally the optimal position and alignment of the peak are measured on the low mass shoulder to avoid tailing from O_2 and negative background due to possible ion scattering on the sides of the Faraday cups.[11,12,25] Fu *et al.*[17] suggested that the addition of N_2 to the central gas flow can greatly suppress oxide polyatomic interferences in the measurement of sulfur isotopes and significantly improve the mass bias stability zone at the optimum makeup gas flow rate. Approximately 4 mL min^{-1} N_2 gas flow rate was applied in this analytical procedure employing pseudo low resolution for the Nu Plasma II MC-ICP-MS. The latter procedure did indeed suppress production of oxide polyatomic interferences for sulfate as shown in Fig. 1, since broad and flat interference-free plateaus for the three sulfur isotopes are recorded and are similar to those observed for the sulfur ion signals measured with the Neptune MC-ICP-MS instrument.[17]

Characterization of reference material. As stated earlier, use of an isotopically homogeneous, matrix-matched mineral reference is important for in-situ sulfur isotopic characterization of barite using SSB. To evaluate the isotopic homogeneity of potential sulfate reference materials and the repeatability of sulfur isotope ratio measurements (both by LA-MC-ICP-MS and EA-IRMS), repeat analyses of the sulfur isotopic composition of natural YF-2 barite were performed. For EA-IRMS analysis, measurement repeatability is defined by the standard deviation of multiple measurements for variable fractions from a bulk sample. The three repeated analyses for one fraction of the bulk YF-2 barite yields a $\delta^{34}S$ value of 18.31± 0.06‰ (2SD) determined at CAS. The analyses of 11 fractions from the bulk YF-2 barite gives a weighted average $\delta^{34}S$ value of 18.1 ± 0.4‰ (2SD) determined at CUG. These $\delta^{34}S$ values are consistent with each other given their associated external reproducibility. The resulting $\delta^{34}S$ values for the YF-2 barite using itself as the

reference material, obtained by LA-MC-ICP-MS on different analytical days using both laser systems, are given in Fig. 2a. The sulfur isotopic composition for YF-2 yields a weighted average $\delta^{34}S$ value of 18.1 ± 0.4‰ (2SD) and 18.0 ± 0.4‰ (2SD) using the RESOlution laser and the GeoLasHD laser, respectively. Sulfur isotopic determination by EA-IRMS and LA-MC-ICP-MS validates the isotopic homogeneity of the YF-2 barite on the bulk and the micron scale. Thus, in this study, the isotopically homogeneous YF-2 barite has been adopted as the reference material for sulfur isotopic determination of barite, which can also be considered as a new isotopic reference material.

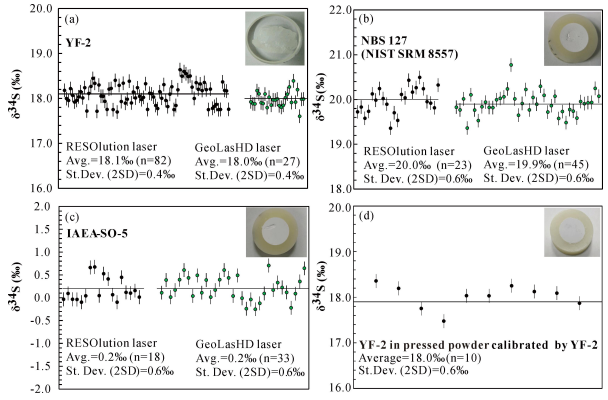

Fig. 2 $\delta^{34}S$ values of YF-2 barite and barium sulfate. (a) Determined $\delta^{34}S$ values of YF-2 barite on different days of analysis. (b) and (c) $\delta^{34}S$ values of barium sulfate calibrated using YF-2 in pressed powder as reference material. (d) YF-2 in pressed powder calibrated using YF-2 as reference material. The black solid lines represent the average value. The error bars are at 2SD level.

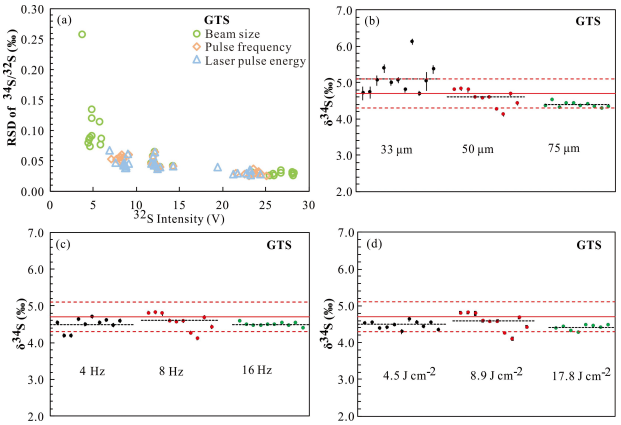

Fig. 3 $\delta^{34}S$ values and the correlation of relative standard deviation of $^{34}S/^{32}S$ and the ^{32}S ion signal intensity of magmatic barite (GTS). (a) shows the correlation of relative standard deviation associated with $^{34}S/^{32}S$ ratios and the ^{32}S ion signal intensity for GTS barite. (b)–(d) display the effect of varying laser ablation parameters with the RESOlution system on sulfur isotope fractionation using the GTS barite. The black dashed lines represent the average value. The red solid lines represent the average value obtained by EA-IRMS and the red dashed lines represent standard deviation range (2SD).

Sulfur isotopic determination of barium sulfate standards. The sulfur isotopic composition of the NBS 127 and IAEA-SO-5 barium sulfate standards was verified by LA-MC-ICP-MS using YF-2 barite. The barium sulfate and the YF-2 barite were made into pressed powder tablets. During laser ablation, the ion signal intensity drops quickly for sulfate in the pressed powder tablet compared to the natural sulfate mineral. Nevertheless, the long-term measurement of the $\delta^{34}S$ ratios for NBS 127 and IAEA-SO-5 using both laser systems agree well with the recommended values using YF-2 in a pressed powder tablet as the bracketing standard (Fig. 2b, c and Table 3). When the YF-2 barite crystal was analyzed with YF-2 barite prepared as a pressed powder tablet, no significant isotopic fractionation was identified between these two samples (Fig. 2d and Table 3).

Sulfur isotopic determination of barite. A selection of barite grains from different geological settings was analyzed by EA-IRMS to characterize their bulk sulfur isotopic compositions as shown in Table 4. For the investigated barites, the sulfur isotopic compositions for the WC and YF-1 barites for several sample fractions determined at the CUG laboratory display larger than expected external reproducibility (> 0.5‰; 2SD; Table 4); therefore, the scale of the isotopic heterogeneity was further verified at the CAS laboratory. The repeated sulfur isotope analyses (n = 3) obtained at CAS from one small barite fraction (approximately 100 mg) for YF-1 show limited sulfur isotopic variation since it is characterized by an external reproducibility of 0.04‰ (2SD). In contrast, WC barite displays a much larger sulfur isotopic variation since it is defined by a larger external reproducibility of 0.42‰ (2SD; Table 4). Thus, these results suggest that WC barite is possibly isotopically heterogeneous at the micron scale.

The $\delta^{34}S$ values for these barite grains were measured by LA-MC-ICP-MS using YF-2 barite as the reference material and the SSB approach. A number of laser ablation parameters are believed to have an effect on the measurement of $\delta^{34}S$

Table 3. $\delta^{34}S$ Values Measured for Barium Sulfate Calibrated by YF-2 Pressed Powder

		$\delta^{34}S$ ± 2SD (‰)		
Sample type	**Sample ID**	**LA (RESOlution laser)-MC-ICP-MS**	**LA (GeoLasHD laser)-MC-ICP-MS**	**Recommended values**
Barium sulfate	NBS 127 (NIST SRM 8557)	20.0 ± 0.6 (n = 23)	19.9 ± 0.6 (n = 45)	20.3[a]
Barium sulfate	IAEA-SO-5	0.2 ± 0.6 (n = 18)	0.2 ± 0.6 (n = 33)	0.5[b]
Barite	YF-2	18.0 ± 0.6 (n = 10)		

[a] Mason et al.[19]; [b] Information from the IAEA reference material certificates.

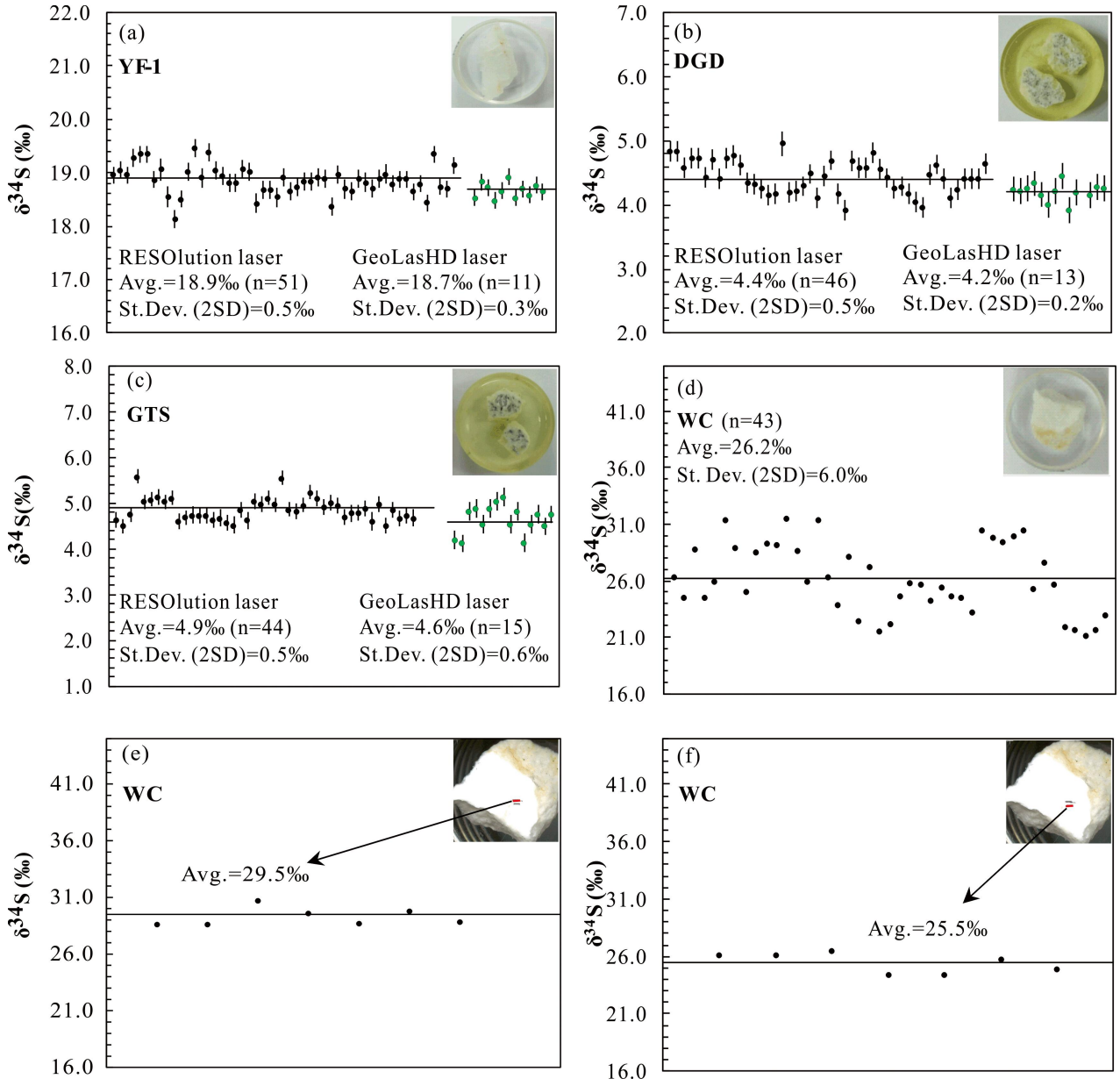

Fig. 4 $\delta^{34}S$ values of barites calibrated using YF-2 as reference material. The black solid lines represent the average value. The error bars are at 2SD level.

Table 4. $\delta^{34}S$ Measured for Sulfate Minerals Using LA-MC-ICP-MS and EA-IRMS

			$\delta^{34}S \pm 2SD$ (‰)			
Sample type	**Matrix**	**Sample ID**	**LA (RESOlution laser)-MC-ICP-MS**	**LA (GeoLasHD laser)-MC-ICP-MS**	**EA-IR-MS (BGEG, CUG)**	**EA-IR-MS (IGSNRR, CAS)**
		YF-2	18.1 ± 0.4 (n =82)	18.0 ± 0.4 (n = 27)	18.1 ± 0.4 (n = 11)	18.31 ± 0.06 (n = 3)
		YF-1	18.9 ± 0.5 (n = 51)	18.7 ± 0.3 (n = 11)	18.5 ± 0.7 (n = 6)	19.00 ± 0.04 (n = 3)
Barite	$BaSO_4$	WC	26.2 ± 6.0 (n = 43)	/	26.4 ± 1.1 (n = 6)	27.19 ± 0.42 (n = 3)
		DGD	4.4 ± 0.5 (n = 46)	4.2 ± 0.2 (n = 13)	4.4 ± 0.2 (n = 5)	/
		GTS	4.9 ± 0.5 (n = 44)	4.6 ± 0.6 (n = 15)	4.7 ± 0.4 (n = 8)	/
Barytocelestine	$(Sr,Ba)SO_4$	DSG	3.7 ± 0.6 (n = 43)	4.0 ± 0.4 (n = 10)	4.0 ± 0.3 (n = 6)	3.25 ± 0.06 (n = 3)
Celestine	$SrSO_4$	BK	5.8 ± 0.4 (n = 30)	6.0 ± 0.5 (n = 15)	6.4 ± 0.4 (n = 6)	6.12 ± 0.44 (n = 3)
Anhydrite	$CaSO_4$	LX	29.8 ± 0.5 (n = 30)	30.1 ± 0.6 (n = 29)	29.5 ± 0.4 (n = 3)	30.3 ± 0.1 (n = 3)

Table 5. $\delta^{34}S$ Measured for Sulfate Minerals with Different Laser Ablation Parameters Using LA-MC-ICP-MS

RESOlution laser					
	$\delta^{34}S \pm 2SD$ (‰)			^{32}S intensity (V)	
Operation parameter	**GTS**	**LX**	**YF-2**	**GTS**	**LX**
33 µm, 8 Hz, 8.9 J cm^{-2}	5.1 ± 0.8 (n = 11)	30.2 ± 0.5 (n = 10)	3.9 (n = 14)	5.0 (n = 11)	4.1 (n = 10)
50 µm, 8 Hz, 8.9 J cm^{-2}	4.6 ± 0.5 (n = 10)	29.7 ± 0.5 (n = 10)	11.9 (n = 6)	12.4 (n = 10)	8.9 (n = 10)
75 µm, 8 Hz, 8.9 J cm^{-2}	4.4 ± 0.1 (n = 10)	29.3 ± 0.3 (n = 9)	27.3 (n = 4)	26.5 (n = 10)	17.5 (n = 9)
50 µm, 4 Hz, 8.9 J cm^{-2}	4.5 ± 0.3 (n = 10)	30.0 ± 0.7 (n = 10)	7.1 (n = 5)	8.2 (n = 10)	4.1 (n = 10)
50 µm, 16 Hz, 8.9 J cm^{-2}	4.5 ± 0.1 (n = 10)	29.3 ± 0.1 (n = 10)	24.1 (n = 4)	23.6 (n = 10)	14.5 (n = 9)
50 µm, 8 Hz, 4.5 J cm^{-2}	4.5 ± 0.2 (n = 11)	29.8 ± 0.5 (n = 10)	8.1 (n = 5)	8.5 (n = 11)	5.5 (n = 10)
50 µm, 8 Hz, 17.8 J cm^{-2}	4.4 ± 0.1 (n = 8)	29.4 ± 0.2 (n = 8)	25.0 (n = 3)	22.4 (n = 8)	12.2 (n = 8)
GeoLasHD laser					
	$\delta^{34}S \pm 2SD$ (‰)			^{32}S intensity (V)	
Operation parameter	**BK**	**LX**	**YF-2**	**BK**	**YF-2**	**LX**
32 µm, 5 Hz, 5 J cm^{-2}	6.1 ± 0.4 (n = 8)	30.0 ± 0.4 (n = 11)	2.3 (n = 5)	2.0 (n = 8)	2.5 (n = 5)	1.4 (n = 11)
60 µm, 5 Hz, 5 J cm^{-2}	6.0 ± 0.5 (n = 9)	30.1 ± 0.2 (n = 10)	5.8 (n = 5)	4.7 (n = 9)	4.4 (n = 5)	5.0 (n = 10)
90 µm, 5 Hz, 5 J cm^{-2}	6.0 ± 0.2 (n = 3)	30.3 ± 0.3 (n = 4)	13.1(n = 3)	12.1 (n = 3)	10.1 (n = 4)	11.7 (n = 4)
60 µm, 10 Hz, 5 J cm^{-2}	6.1 ± 0.1 (n = 3)	30.1 ± 0.2 (n = 10)	12.0 (n = 3)	11.0 (n = 3)	8.5 (n = 4)	9.1 (n = 10)
60 µm, 15 Hz, 5 J cm^{-2}	/	30.2 ± 0.4 (n = 11)	/	/	11.0 (n = 6)	12.5 (n = 11)
60 µm, 5 Hz, 8 J cm^{-2}	6.1 ± 0.04 (n = 3)	30.4 ± 0.4 (n = 4)	13.8 (n = 2)	10.2 (n = 3)	8.3 (n = 4)	7.6 (n = 4)
32 µm, 5 Hz, 5 J cm^{-2}	6.1 ± 0.4 (n = 8)	30.0 ± 0.4 (n = 11)	2.3 (n = 5)	2.0 (n = 8)	2.5 (n = 5)	1.4 (n = 11)
32 µm, 5 Hz, 16 J cm^{-2}	5.8 ± 0.2 (n = 8)	29.9 ± 0.6 (n = 4)	6.9 (n = 5)	6.0 (n = 8)	7.0 (n = 4)	4.4 (n = 8)

ratios using the LA-MC-ICP-MS approach due to documented isotopic fractionation at the laser ablation site.[10,15,18,37,38] By adopting a variable beam size, pulse frequency, and fluence with the RESOlution laser system, the recorded ion signal intensities of ^{32}S for the GTS barites varied from approximately 3 to 30 V (Fig. 3a). As shown in Fig. 3a, the relative standard deviation (RSD) associated with the measured $^{34}S/^{32}S$ ratios shows a negative correlation with the ^{32}S ion signal intensity. The RSD associated with the measured $^{34}S/^{32}S$ ratios increases significantly when the ^{32}S ion signal intensity is < 8 V, whereas it decreases and becomes relatively stable with ^{32}S ion signals > 20 V (Fig. 3a). The variability of the ^{32}S ion signal intensity was changed by adopting a different ablation spot size, frequency, or fluence. Thus, the high RSD at low ^{32}S ion signal intensity using smaller spot size could be due to a small-scale isotopic heterogeneity in the sample or an increased downhole fractionation, and at low fluence it could mean that the sample is not ablating well and larger-sized particles are formed, resulting in a noisy signal. Nevertheless, a sulfur ion signal intensity > 5 volts results in lower relative standard deviation of the measured $^{34}S/^{32}S$ ratios (Fig. 3a).

Various laser ablation parameters were tested to verify their effects on the $\delta^{34}S$ characterization of barite. The $\delta^{34}S$ values for GTS with YF-2 barite external normalization were determined with variable beam sizes of 33 µm, 50 µm, and 75 µm, whereas other parameters remained constant in the RESOlution laser system (e.g., pulse frequency of 8 Hz, fluence of 8.9 J cm^{-2}). Sulfur ion signal intensities recorded at 75 µm were approximately two times higher than at 50 µm, and five times higher than at 33 µm for the GTS and YF-2 barite reference materials (Table 5). The external reproducibility decreased with increasing beam size (Fig. 3b), and the $\delta^{34}S$ value also decreased from 5.0 ± 0.8‰ to 4.4 ± 0.1‰ with an increase in the ion beam intensity. All of the sulfur isotopic compositions determined by LA-MC-ICP-MS corroborate those obtained by EA-IRMS, given their associated external reproducibility (Fig. 3b). In this study, a beam size of 50 µm is preferred for the sulfur isotopic determination of barite since the results best agreed with the EA-IRMS average value and represents a compromise between satisfactory analytical precision and desired spatial resolution. GTS barite together with YF-2 barite as the bracketing standard were further analyzed with varied laser ablation pulse frequencies (4 Hz, 8 Hz, and 16 Hz) and fluences (4.5 J cm^{-2}, 8.9 J cm^{-2}, and 17.8 J cm^{-2}). Since the calculated $\delta^{34}S$ values for GTS barite were relatively consistent (Fig. 3c, d), the frequency of 8 Hz and a corresponding fluence of 8.9 J cm^{-2} were deemed to be the preferred laser settings for this study.

Adopting these preferred laser ablation parameters cited above, the $\delta^{34}S$ values for the YF-1, DGD, GTS and WC barites were determined using YF-2 as the bracketing standard for both laser systems. The $\delta^{34}S$ ratios for YF-1, DGD and GTS using the RESOlution laser system agree well with the EA-IRMS determined compositions, while they were a bit lower when using the GeoLasHD laser but also within standard deviation. In general, they are both characterized by acceptable precision (~0.5‰, 2SD; Fig. 4a–c; Table 4). The weighted average $\delta^{34}S$ for WC barite is associated with a large

external reproducibility of 6.0‰ (2SD) which confirms isotopic heterogeneity (Table 4; Fig. 4d). Nevertheless, the weighted mean $\delta^{34}S$ value for WC barite is consistent to the value determined by EA-IRMS. Repeated ablation of different domains on the WC barite crystal generated different sulfur isotopic compositions that ranged from 21‰ to 31.5‰. As shown in Fig. 4e and 4f, two different domains of the WC barite are characterized by distinct $\delta^{34}S$ compositions at 29.4‰ and 25.5‰, respectively. Hence, the difference between the average sulfur isotopic composition determined by LA-MC-ICP-MS for WC barite and its counterpart value obtained by EA-IRMS may be related to sample isotopic heterogeneity and hence, most likely does not represent the analysis of identical fractions. Combined with the EA-IRMS analyses, the WC barite indicates large sulfur isotopic fractionation at the micron scale, which possibly suggests varying conditions or source heterogeneity during its formation.

Matrix effects between sulfates using the RESOlution laser. Laser parameters, gas conditions, and mechanical characteristics of the sample can influence isotopic fractionation during LA-MC-ICP-MS analysis. Isotopic fractionation occurs at the laser ablation site due to the melting caused by laser heating and varied particle size distributions.[18,39] The matrix-induced mass bias for sulfur isotopic determination by LA-MC-ICP-MS was tested between sulfide (e.g., WS-1 pyrite) and sulfate (YF-2 barite). The recorded sulfur isotope signals for barite are much smoother (less transient) than those for pyrite during the entire ablation interval with the same laser parameters employed (Fig. 5a, b). The significant drop in the sulfur ion signal intensities during the ablation of pyrite is possibly due to reduced transport efficiency and the presence of abundant debris generated during the ablation or an ablation rate difference for the sulfides versus the sulfate matrices.[16,18] The $^{34}S/^{32}S$ ratios for pyrite and barite behaved similarly through the ablation interval, thus no significant downhole fractionation was observed (Fig. 5a, b). Moreover, the $\delta^{34}S$ values indicate that the matrix-induced isotopic fractionation effect between pyrite and barite is highly variable within a single analytical session (Fig. 5c). The matrix effect can be reduced or even eliminated when the ablation system and MC-ICP-MS are operating at optimal conditions (e.g., stable after 2 hours due to the air in the sample chamber and laser cell being effectively flushed).

Lighter $\delta^{34}S$ values have been reported for NBS 127 barite using sulfide as the reference material, with values between −1.8 and −2.5‰.[13] Mason *et al.*[19] suggested that sulfur isotopic determination in NBS 127 sulfate was less accurate when calibrated against IAEA-S sulfides. Pribil *et al.*[16] reported the difference of sulfur isotopic fractionation behavior for sulfate and sulfide, which were attributed to a non-spectral sulfur oxidation effect.

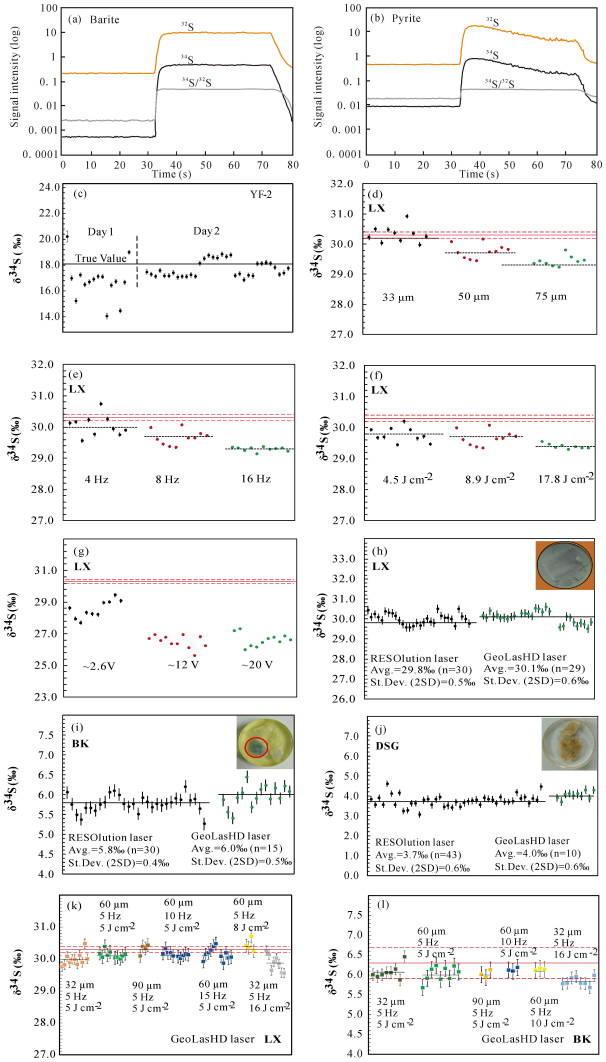

Fig. 5 (a) and (b) illustrate sulfur isotope signals during ablation of barite and pyrite. (c) YF-2 barite using pyrite as reference material. (d)–(f) display the results of sulfur isotope fractionation for LX anhydrite as a function of beam size (d), laser pulse rate (e) and laser fluence (f). (g) displays the results of sulfur isotope fractionation with matched ion signal intensity between reference material and sample. The corresponding laser ablation parameters used for YF-2 and LX are shown in Table 6. (h)–(j) $\delta^{34}S$ values of LX anhydrite, BK celestine and DSG barytocelestine. (k) and (l) The effects of varying GeoLasHD laser ablation parameters on sulfur isotope fractionation. The black solid lines represent the average value. The red solid lines represent the average value obtained by EA-IRMS and the red dashed lines represent deviation range. The error bars are at 2SD level.

The effects of laser beam size, pulse frequency, and fluence for the RESOlution laser system were investigated with the analysis of LX anhydrite with YF-2 barite as the reference material. The $\delta^{34}S$ values for LX anhydrite determined at varied beam sizes are shown in Table 5 and Fig. 5d. For all beam sizes employed, the degree of sulfur isotopic fractionation is essentially negligible (total variation is within the external reproducibility); however, the $\delta^{34}S$ value

determined based on the results for the 33 μm beam size overlaps that determined for the bulk sulfur isotopic composition. The sulfur isotopic composition for LX anhydrite determined with a beam size of 75 μm was −0.9‰ lower compared to the value obtained with ablations using the 33 μm beam size (Table 5, Fig. 5d). Similar behavior was observed in the sulfur isotopic determination for pyrite, boron and lithium isotope analysis in silicate glasses and minerals using LA-MC-ICP-MS,[15,18,39] which suggests that different beam sizes can lead to isotopic fractionation at the laser ablation site with smaller beam sizes yielding more accurate results.

Sulfur isotopic compositions for LX anhydrite using YF-2 barite as reference material were determined with varied laser ablation pulse frequencies (4 Hz, 8 Hz, and 16 Hz), which indicate slight isotopic fractionation. For instance, the offsets in $\delta^{34}S$ values were approximately −0.4‰ with a pulse frequency of 8 Hz, and −0.8‰ with a pulse frequency of 16 Hz compared to the $\delta^{34}S$ value obtained with a pulse frequency of 4 Hz (Fig. 5e). Of note, $\delta^{34}S$ value for LX anhydrite ablated at 4 Hz shows the smallest difference compared to that determined by EA-IRMS (Table 5). In other words, adopting a lower ablation pulse frequency results in smaller matrix-induced isotopic fractionation between anhydrite and barite. This feature is similar to that previously observed for in-situ Mg isotopic determinations conducted by Norman *et al*.[40]

Similarly, laser fluence is also an important ablation parameter that possibly contributes to isotopic fractionation at the ablation site. Of note, the sulfur ion signals recorded when using the laser fluence of 17.8 J cm^{-2} and 8.9 J cm^{-2} were generally 3 times and 2 times higher, respectively, than that at 4.5 J cm^{-2} for both LX anhydrite and barites (Table 5). These data suggest that the transport efficiency of sulfur is lower when using a higher laser fluence. This may be attributed to melting the sample during ablation, or part of the sulfur is converted into a gas phase rather than transporting all of the sulfur as particles to the plasma. If sulfur is transported as a gas, then there may be a loss in transport efficiency since gas behaves differently in the plasma environment compared to particle phase. Using variable laser fluence output again affects sulfur isotopic composition for anhydrite (*e.g.* LX) and high fluence (i.e., 17.8 J cm^{-2}) results in −0.4‰ compared to that at 4.5 J cm^{-2} (Table 5; Fig. 5f). The different behavior for barite and anhydrite using the RESOlution laser might be the result of laser fluence-induced melting effect as the melting temperature of barite (1580 °C) is higher than that of anhydrite (1460 °C). Reducing laser fluence output also slightly minimizes the matrix effect for anhydrite when using barite as reference material, a similar feature was noted with decreasing laser repetition rate (Fig. 5f; Table 5).

Table 6. $\delta^{34}S$ Measured for Sulfate Minerals with Matched Signal Intensity using LA-MC-ICP-MS

Operation parameter		^{32}S intensity (V)		$\delta^{34}S$ ± 2SD (‰)
YF-2	**LX**	**YF-2**	**LX**	**LX**
50 μm, 4 Hz, 8.9 J cm^{-2}	50 μm, 10 Hz, 8.9 J cm^{-2}	2.6	2.5	28.6 ± 1.2 (n = 10)
75 μm, 8 Hz, 8.9 J cm^{-2}	75 μm, 10 Hz, 17.8 J cm^{-2}	12.0	11.7	26.5 ± 0.8 (n = 11)
75 μm, 8 Hz, 17.8 J cm^{-2}	90 μm, 12 Hz, 8.9 J cm^{-2}	21.0	20.5	26.5 ± 0.6 (n = 11)

Of interest, when using the same laser ablation parameters, the recorded sulfur ion signal intensities are different between non-barite sulfates and barite. For instance, the ^{32}S ion signal intensity for barite is 25.0 V, which is almost twice the intensity recorded for anhydrite (12.2 V) when adopting a beam size of 50 μm, frequency of 8 Hz, and fluence of 17.8 J cm^{-2}. Pribil *et al*.[16] suggested that sulfur isotopic mass fractionation can be induced within the plasma, which was potentially related to the oxidation state of sulfur and this, in turn, may affect its behavior in the plasma during vaporization and atomization. Chen *et al*.[26] indicated that the sulfate and nitrate concentration can affect the vaporization and ionization efficiency and ionization position, which results in instrument-induced sulfur isotopic fractionation. The ^{32}S signals recorded for the barite reference material and LX anhydrite were matched in order to verify if the observed fractionation cited above and is a result of plasma loading rather than a laser-induced fractionation. The results indicate that isotopic fractionation is still present when the ^{32}S ion signal intensities for the sample and the reference material are similar (Table 6 and Fig. 5g). High ion signal intensity (e.g. 20.5 V of ^{32}S) results in −5.3‰ difference for LX anhydrite, which is much higher compared to that (−3.2‰) at low signal intensity (~2.6 V). Thus, it is plausible that isotopic fractionation happens both at the ablation site/sample chamber and in the plasma.

As a compromise in relation to both accuracy and precision, a moderate beam size (50 μm), frequency (8 Hz), and fluence (8.9 J cm^{-2}) were adopted for laser ablation runs. When using the latter conditions, the measured $\delta^{34}S$ values for the non-barite sulfate including LX anhydrite, BK celestine, and DSG barytocelestine were all similar to those obtained by EA-IRMS (Fig. 5h–j).

Matrix effects between sulfates using the GeoLasHD laser. We also performed matrix effect investigations on sulfur isotopic determinations using the new GeoLasHD laser by analyzing LX anhydrite, BK celestine, and DSG barytocelestine, with YF-2 barite as the reference material. No obvious sulfur isotopic fractionation was observed when using different laser parameters during the ablation experiments, and the in-situ sulfur isotopic compositions were consistent

with those obtained by bulk methods (Table 5 and Fig. 5h–l). Moreover, when using the GeoLasHD laser system, the measured sulfur ion signal intensities were similar between non-barite sulfates (*e.g.* anhydrite and celestine) and barite with the same laser ablation parameters (Table 5). In this study, the yielded ^{32}S intensity was coordinated among barite and non-barite sulfate of different laser parameters using the GeoLasHD laser, whereas they were not coordinated using the RESOlution laser. The differences between RESOlution and GeoLas might be due to a different energy distribution in the laser beam. Thus, coordination between ion signal intensity of the target isotope and laser parameters is important for non-matrix matched sulfur isotopic analysis.

CONCLUSIONS

Sulfur isotopic compositions were assessed for a selected number of sulfate minerals with the aim of presenting preliminary data for potential new sulfate reference materials to be used by the geological community. YF-2 barite is homogeneous and may be adopted as a reference material for sulfur isotopic determinations. Using the standard-sample-bracketing approach, the sulfur isotopes of NBS 127 and IAEA-SO-5 barium sulfate by using YF-2 pressed powder tablets as a reference material yielded consistent results that compare well with their recommended values. The external reproducibility associated with the $\delta^{34}S$ values based on repeated analyses of natural barite (with the exception of isotopically heterogeneous WC barite) by LA-MC-ICP-MS is estimated to be at 0.5‰ (2SD). The values of $\delta^{34}S$ for barite obtained by LA-MC-ICP-MS are equivalent to those obtained by EA-IRMS. The possible matrix effects between barite and non-barite sulfates in the determinations of sulfur isotopic compositions are considered negligible when using both laser ablation systems employed here. Coordination between signal intensity of the target isotope and the laser parameters are important for non-matrix matched sulfur isotopic analysis. When fractionation is observed, employing a smaller beam size, lower repetition rate, and fluence output can help to minimize isotopic fractionation during ablation.

AUTHOR INFORMATION

Corresponding Author

*W. Chen

Email address: wchen@cug.edu.cn

Notes

The authors declare no competing financial interest.

ACKNOWLEDGMENTS

Liu Yan from Institute of Geology, Chinese Academy of Geological Sciences, is warmly thanked for providing the sulfate sample from Maoniuping deposit. We acknowledge help in the sulfur isotopic determination by EA-IRMS offered by Zihu Zhang and Professor Chao Li from the China University of Geosciences (Wuhan) and Dr. Liyan Tian and Professor Qingjun Guo from the Institute of Geographic Sciences and Natural Resources Research, Chinese Academy of Sciences. This study was supported by the National Key R&D Program of China (2016YFE0203000), National Natural Science Foundation of China (Nos. 41530211, 41673035), the 111 Project (BP0719022), the Fundamental Research Funds for the Central Universities (CUGCJ1709) and the special fund from the State Key Laboratory of Geological Processes and Mineral Resources (MSFGPMR03-2).

REFERENCES

1. R. R. Seal, C. N. Alpers, and R. O. Rye, *Rev. Mineral. Geochem.*, 2000, **40**, 541–602. https://doi.org/10.2138/rmg.2000.40.12
2. N. V. Grassineau, D. P. Mattey, and D. Lowry, *Anal. Chem.*, 2001, **73**, 220–225. https://doi.org/10.1021/ac000550f
3. J. Hoefs, *Stable Isotope Geochemistry*. Cham: Springer International Publishing, 2015. https://doi.org/ 10.1007/978-3-319-19716-6
4. L. Marini, R. Moretti, and M. Accornero, *Rev. Mineral. Geochem.*, 2011, **73**, 423–492. https://doi.org/10.2138/rmg.2011.73.14
5. A. Pellerin, T. H. Bui, M. Rough, A. Mucci, D. E. Canfield, and B. A. Wing, *Geochim. Cosmochim. Acta*, 2015, **149**, 152–164. https://doi.org/10.1016/j.gca.2014.11.007
6. C. E. Rees, W. J. Jenkins, and J. Monster, *Geochim. Cosmochim. Acta*, 1978, **42**, 377–381. https://doi.org/10.1016/0016-7037(78)90268-5
7. R. R. Seal, *Rev. Mineral. Geochem.*, 2006, **61**, 633–677. https://doi.org/10.2138/rmg.2006.61.12
8. A. Giesemann, H. J. Jäger, A. L. Norman, H. R. Krouse, and W. A. Brand, *Anal. Chem.*, 1994, **66**, 2816–2819. https://doi.org/10.1021/ac00090a005
9. S. A. Studley, E. M. Ripley, E. R. Elswick, M. J. Dorais, J. Fong, D. Finkelstein, and L. M. Pratt, *Chem. Geo.*, 2002, **192**, 141–148. https://doi.org/10.1016/s0009-2541(02)00162-6
10. C. Bendall, Y. Lahaye, J. Fiebig, S. Weyer, and G. P. Brey, *Appl. Geochem.*, 2006, **21**, 782–787. https://doi.org/10.1016/j.apgeochem.2006.02.012
11. R. Clough, P. Evans, T. Catterick, and E. H. Evans, *Anal. Chem.*, 2006, **78**, 6126–6132. https://doi.org/10.1021/ac060875h
12. P. R. Craddock, O. J. Rouxel, L. A. Ball, and W. Bach, *Chem. Geol.*, 2008, **253**, 102–113. https://doi.org/10.1016/j.chemgeo.2008.04.017
13. B. Bühn, R. V. Santos, M. A. Dardenne, and C. G. de Oliveira, *Chem. Geol.*, 2012, **312–313**, 163–176. https://doi.org/10.1016/j.chemgeo.2012.04.003

14. B. R. Berger, R. W. Henley, H. A. Lowers, and M. J. Pribil, *J. Volcanol. Geotherm. Res.*, 2014, **271**, 70–82. https://doi.org/10.1016/j.jvolgeores.2013.11.019
15. S. E. Gilbert, L. V. Danyushevsky, T. Rodemann, N. Shimizu, A. Gurenko, H. Meffre Thomas, R. R. Large, and D. Death, *J. Anal. At. Spectrom.*, 2014, **29**, 1042–1051. https://doi.org/10.1039/c4ja00011k
16. M. J. Pribil, W. I. Ridley, and P. Emsbo, *Chem. Geo.*, 2015, **412**, 99–106. https://doi.org/10.1016/j.chemgeo.2015.07.014
17. J. Fu, Z. Hu, W. Zhang, L. Yang, Y. Liu, M. Li, K. Zong, S. Gao, and S. Hu, *Anal. Chim. Acta*, 2016, **911**, 14–26. https://doi.org/10.1016/j.aca.2016.01.026
18. Z. Y. Zhu, S. Y. Jiang, C. L. Ciobanu, T. Yang, and N. J. Cook, *Chem. Geo.*, 2017, **450**, 223–234. https://doi.org/10.1016/j.chemgeo.2016.12.037
19. P. R. D. Mason, J. Košler, J. C. M. de Hoog, P. J. Sylvester, and S. Meffan-Main, *J. Anal. At. Spectrom.*, 2006, **21**, 177–186. https://doi.org/10.1039/b510883g
20. A. E. Williams-Jones, I. M. Samson, and G. R. Olivo, *Econ. Geol.*, 2000, **95**, 327–341. https://doi.org/10.2113/gsecongeo.95.2.327
21. J. S. Hanor, *Rev. Mineral. Geochem.*, 2019, **40**, 193–275. https://doi.org/10.2138/rmg.2000.40.4
22. D. J. Kontak, K. Kyser, A. Gize, and D. Marshall, *Econ. Geol.*, 2006, **101**, 407–430. https://doi.org/10.2113/gsecongeo.101.2.407
23. C. Monnin and D. Cividini, *Geochim. Cosmochim. Acta*, 2006, **70**, 3290–3298. https://doi.org/10.1016/j.gca.2006.04.002
24. M. Rehkämper, M. Schönbächler, and C. H. Stirling, *Geostand. Newsl.*, 2001, **25**, 23–40. https://doi.org/10.1111/j.1751-908x.2001.tb00785.x
25. G. Paris, A. L. Sessions, A. v. Subhas, and J. F. Adkins, *Chem. Geol.*, 2013, **345**, 50–61. https://doi.org/10.1016/j.chemgeo.2013.02.022
26. L. Chen, K. Chen, Z. Bao, P. Liang, T. Sun, and H. Yuan, *J. Anal. At. Spectrom.*, 2017, **32**, 107–116. https://doi.org/10.1039/C6JA00270F
27. Y. Feng, W. Zhang, Z. Hu, Y. Liu, K. Chen, J. Fu, J. Xie, and Q. Shi, *J. Anal. At. Spectrom.*, 2018, **33**, 2172–2183. https://doi.org/10.1039/c8ja00305j
28. J. Fu, Z. Hu, J. W. Li, L. Yang, W. Zhang, Y. Liu, Q. Li, K. Zong, and S. Hu, *J. Anal. At. Spectrom.*, 2017, **32**, 2341–2351. https://doi.org/10.1039/c7ja00282c
29. S. A. Wilson, W. I. Ridley, and A. E. Koenig, *J. Anal. At. Spectrom.*, 2002, **17**, 406–409. https://doi.org/10.1039/B108787H
30. D. Garbe-Schönberg and S. Müller, *J. Anal. At. Spectrom.*, 2014, **29**, 990–1000. https://doi.org/10.1039/c4ja00007b
31. S. Tian, T. Ding, J. Mao, L. I. Yanhe, and Z. Yuan, *Acta Geol. Sin. (Engl. Ed.)*, 2010, **80**, 540–549. https://doi.org/10.1111/j.1755-6724.2006.tb00274.x
32. W. Song, C. Xu, M. P. Smith, J. Kynicky, K. J. Huang, C. W. Wei, L. Zhou, and Q. H. Shu, *Sci. Rep.*, 2016, **6**, 37377. https://doi.org/10.1038/srep37377
33. T. B. Coplen and H. R. Krouse, *Nature*, 1998, **392,** 32–32. https://doi.org/10.1038/32080
34. T. Ding, S. Valkiers, H. Kipphardt, P. De Bievre, P. D. P. Taylor, R. Gonfiantini, and R. Krouse, *Geochim. Cosmochim. Acta*, 2001, **65**, 2433–2437. https://doi.org/10.1016/s0016-7037(01)00611-1
35. X. Han, Q. Guo, H. Strauss, C.Q. Liu, J. Hu, Z. Guo, R. F. Wei, M. Peters, L. Y. Tian, and J. Kong, 2017, *Environ. Sci. Technol.,* **51**, 7794–7803. https://doi.org/10.1021/acs.est.7b00280
36. J. Giner Martínez-Sierra, O. Galilea San Blas, J. M. Marchante Gayón and J. I. García Alonso, *Spectrochim. Acta, Part B*, 2015, **108**, 35–52. http://dx.doi.org/10.1016/j.sab.2015.03.016
37. S. E. Jackson and D. Günther, *J. Anal. At. Spectrom.*, 2003, **18**, 205–212. https://doi.org/10.1039/b209620j
38. J. Košler, R. B. Pedersen, C. Kruber, and P. J. Sylvester, *J. Anal. At. Spectrom.*, 2005, **20**, 192–199. https://doi.org/10.1039/b412169d
39. J. I. Kimura, Q. Chang, T. Ishikawa, and T. Tsujimori, *J. Anal. At. Spectrom.*, 2016, **31**, 2305–2320. https://doi.org/10.1039/c6ja00283h
40. M. D. Norman, M. T. McCulloch, H. S. C. O'Neill, and G. M. Yaxley, *J. Anal. At. Spectrom.*, 2006, **21**, 50–54. https://doi.org/10.1039/b510719a